Experimental Mechanics (2021) 61:461–468
https://doi.org/10.1007/s11340-020-00677-3

BRIEF TECHNICAL NOTE

Dynamic Tensile Response of a Microwave Damaged Granitic Rock

X. Li[1,2] · S. Wang[1] · K. Xia[1,2] · T. Tong[3]

Received: 11 June 2020 / Accepted: 19 October 2020 / Published online: 23 November 2020

Abstract

Background Understanding the dynamic tensile response of microwave damaged rock is of great significance to promote the development of microwave-assisted hard rock breakage technology. However, most of the current research on this issue is limited to static loading conditions, which is inconsistent with the dynamic stress circumstances encountered in real rock-breaking operations.

Objective The objective of this work is to investigate the effects of microwave irradiation on the dynamic tensile strength, full-field displacement distribution and average fracture energy of a granitic rock.

Methods The split Hopkinson pressure bar (SHPB) system combined with digital image correlation (DIC) technique is adopted to conduct the experiments. The overload phenomenon, which refers to the strength over-estimation phenomenon in the Brazilian test, is validated using the conventional strain gauge method. Based on the DIC analysis, a new approach for calculating the average fracture energy is proposed.

Results Experimental results show that both the apparent and true tensile strengths increase with the loading rate while decreasing with the increase of the irradiation duration; and the true tensile strength after overload correction is lower than the apparent strength. Besides, the overload ratio and fracture energy also show the loading rate and irradiation duration dependency.

Conclusions Our findings prove clearly that microwave irradiation significantly weakens the dynamic tensile properties of granitic rock.

Keywords Microwave irradiation · SHPB · Dynamic tensile response · Digital image correlation (DIC) · Overload correction · Average fracture energy

Introduction

Microwave-assisted hard rock breakage has been considered as a promising technique to reduce the cutter wear and energy consumption when tunnelling in hard rock formations [1–4]. To better illustrate the weakening effect of microwave irradiation, numerous experimental studies have been conducted using different rocks such as ilmenite [5], granodiorite [6], basalt [7], gabbro [8], granite and sandstone [9, 10]. Generally, the microwave-induced damage within the rocks results in rock strength reduction and thus facilitates hard rock breakage. Since rocks are considerably weaker in tension than in compression, an accurate understanding of the tensile response of microwave damaged rock is more crucial. However, the existing investigations on this issue are mainly focused on the tensile properties variation due to microwave irradiation under static stress conditions [2–4, 7], which are inconsistent with the dynamic stress circumstances encountered in real rock-breaking operations [11]. Under dynamic loading conditions, the tensile properties of rocks are quite different from those under static loading [12–14], therefore, it is desirable to investigate the dynamic tensile response of microwave damaged rock. In this work, the dynamic Brazilian disc (BD) tests were conducted using a split Hopkinson pressure bar (SHPB) system in conjunction with the digital image correlation (DIC) technique [15]. The overload effect [16], a phenomenon where the tensile strength is always over-estimated due to the strength being calculated through the peak point of the

✉ K. Xia
kaiwen.xia@utoronto.ca

[1] State Key Laboratory of Hydraulic Engineering Simulation and Safety, School of Civil Engineering, Tianjin University, Tianjin 300072, China

[2] Department of Civil & Mineral Engineering, University of Toronto, Toronto, ON M5S 1A4, Canada

[3] Key Laboratory of Ministry of Education on Safe Mining of Deep Metal Mines, Northeastern University, Shenyang 110819, China

strain curve instead of the value corresponding to the fracture onset, was considered to correct the strength data. Also, the influence of microwave irradiation on the over-estimation ratio was discussed. Based on the velocity characteristics of the splitting fragments deduced from the displacement data, four individual loading stages were discovered, and the fragment movement information was clearly identified. Finally, the fracture energy was calculated and the effects of loading rate and microwave irradiation on average fracture energy were revealed.

Experimental Scheme

Specimen Preparation and Testing System

Fangshan granite (FG), a medium-grained rock, is mainly composed of 59.4% feldspar (by volume) with quartz, annite and greenalite making up most of the rest. Amongst them, the annite and greenalite contain Ferrum which has been proven as strong microwave absorbers [10]. The disc-like specimens were prepared following the International Society for Rock Mechanics and Rock Engineering (ISRM) suggested method [17]. The dimensions of the specimens were 50 mm in diameter and 25 mm in thickness. The prepared specimens were preconditioned by a CM-06S multimode cavity microwave system with a frequency of 2.45 GHz and a power of 6 kW. To avoid the moisture absorbing the microwave energy and further inducing cracking, the specimens were dried in an electrical furnace at 105 °C for 24 h before the microwave treatment. Note that the main crack was observed by unaided eyes and a local melted zone appeared after irradiation for 300 s. Therefore, the irradiation durations were separately set to 0 s, 90 s, 180 s and 270 s.

The dynamic BD tests were performed using a 25.4-mm-diameter SHPB system (Fig. 1) combined with the DIC technique [18–21]. The calculation program employed in this study was Ncorr, which is an open-source code in the MATLAB software [20]. The dimensions of the testing system, details of dynamic force equilibrium achievement and the definition of the loading rate can be found in our previous works [22–24]. A high-speed camera (Photron Fastcam SA1.1) was used to capture the images of the deformed rock surface throughout the test. To minimize the thermal effect on the accuracy of DIC displacement/strain measurement, a LED lamp was placed nearby the camera to provide sufficient luminance on the rock surface. During the dynamic test, the camera was automatically triggered by detecting the pre-set threshold of the incident wave, thereby synchronizing the high-speed camera and the oscilloscope. The resolution of high-speed images in our experiment is 192 × 160 pixels for a frame rate of 120,000 fps, and the corresponding inter-frame time is roughly 7.67 μs. To achieve the optimal speckle pattern, high-contrast black speckles, with an average size ranging from 4 to 5 pixels, were made on the surface of the specimens [25, 26]. The parameters used in the DIC analysis are detailed in Table 1.

Correction for Dynamic BD Tensile Strength

As an indirect method for determining tensile strength, many scholars have pointed out the BD test may overestimate the tensile strength of rocks [27–30]. A probable explanation for this overestimation is the overload phenomenon, in which the cracked specimen can take further load before the final collapse [16]. In a dynamic loading test with a higher loading rate, this overload phenomenon is presumably more serious. It is well known that the Griffith failure criterion is valid at fracture onset, therefore, the correction for the indirect tensile strength is thus critical to dynamic BD tests. Using the method identifying the overload phenomenon proposed by Xia et al. [22], a strain gauge was glued on the surface at the location 5 mm away from the center of each specimen (Fig. 1) to determine the fracture onset. As shown in Fig. 2, the turning point B in the recorded strain signal is caused by the elastic release wave emitted upon crack initiating [31, 32]. By subtracting the propagation time from the moment of the turning point B, the exact time of the primary crack initiation can be obtained, and thus the tensile stress (point C) at that time can be accurately determined. As a result, the BD apparent tensile strength can be corrected to obtain the true tensile strength (the tensile stress at point C shown in Fig. 2). It is noted that the overload ratio is not constant, thus in this work the overload effect was critically assessed for every dynamic Brazilian tensile test.

Results and Discussion

Effects of Microwave Irradiation and Loading Rate on Apparent and Corrected Dynamic Tensile Strength

The consensus for a valid Brazilian tensile test is that the disc should split along the compressive diametric line and the initiation point of the crack should be close to the geometric center [28, 33, 34]. Figure 3(a) illustrates an example of the dynamic test to explain the failure process and tensile strain distribution characteristics during the overall loading process. Twelve points at the specific moments are delimited in the stress-time history curve, and the corresponding snapshots of vertical strain distributions in DIC analysis are displayed in Fig. 3(b). One can see that there is no obvious area of strain concentration occurring at the impacted ends of the specimen before the peak value. As the load increases, the magnitude of strain in the central area is much greater than those at the edges (snapshots $c \sim e$), indicating that the primary crack initiates at

Table 1 Parameters used in the DIC configuration

ROI radius /mm	Subset radius /pixel	Subset spacing /pixel	Norm of the difference vector	Maximum number of iterations	High Strain Analysis	Unit/ Pixel /mm	Strain radius /pixel
23	10	1	1e-7	50	/	0.3005	4

ROI refers to the region of interest in DIC analysis

the disc center along the horizontal diameter. After snapshot *e*, the primary crack gradually propagates towards the supporting points of the bars (snapshots *f*~*k*), and two strain-concentrated zones are formed enclosing the edges (snapshot *l*).

Figure 3(c) presents the dynamic strength versus the loading rate with and without overload correction at different irradiation durations. The tensile strength without overload correction (i.e., the apparent tensile strength) exhibits an approximately linear increasing trend with the increase of the loading rate, whereas it decreases with the increase of the microwave irradiation duration. The relationship between the apparent tensile strength and the irradiation duration is consistent with that in Hassani's work [2]. Specifically, for a given microwave power level, the longer duration of the microwave irradiation, the more microcracks and voids induced, the more reduction of the tensile strength. For similar loading rates, the highest tensile strength (46.28 MPa) occurs at the loading rate of 918 GPa/s without microwave irradiation. While the lowest strength (33.55 MPa) happens at the loading rate of 924 GPa/s with the irradiation duration of 270 s, approximately a 27.5% strength reduction ratio.

Considering the overload correction, we find that the corrected strength is much lower than the corresponding strength calculated by the peak value in the stress-time curve (Fig. 3(c)). In order to quantify the effect of microwave damage and loading rate on the overload, the tensile strength overload ratio (defined as the ratio of the overload to the apparent tensile strength) is introduced in this work. As illustrated in Fig. 3(d), the overload ratio of the tensile strength significantly varies with the increase of the loading rate and irradiation time, i.e., the overload leads to approximately a 15.9% over-estimation of the tensile strength of the raw rock with the loading rate of 1489 GPa/s. Whereas an almost 26.7% over-estimation is observed in the specimen with the irradiation duration of 270 s and a loading rate of 1421 GPa/s. The strength overload ratio shows an obvious increasing trend as the loading rate increases, and the microwave irradiation can enhance the overload percentage of the tensile strength. In addition, for the specimens with longer microwave irradiation durations (i.e., irradiation durations 180 s and 270 s), the increased rate of the strength overload ratio as a function of loading rate is more evident than that under relatively shorter irradiation durations (i.e., irradiation durations 0 s and 90 s).

Effects of Microwave Irradiation and Loading Rate on Average Fracture Energy

The average fracture energy G_c during cracking can be calculated the expression $G_c = (\triangle W\text{-}K_f)/A_c$, where $\triangle W$ is the total energy consumed during dynamic loading which can be directly calculated by the strain history on the bars [35], A_c is the cross-sectional area of the disc, and K_f denotes the residue kinetic energy quantified by $1/2mv^2$. Thus, the key issue for

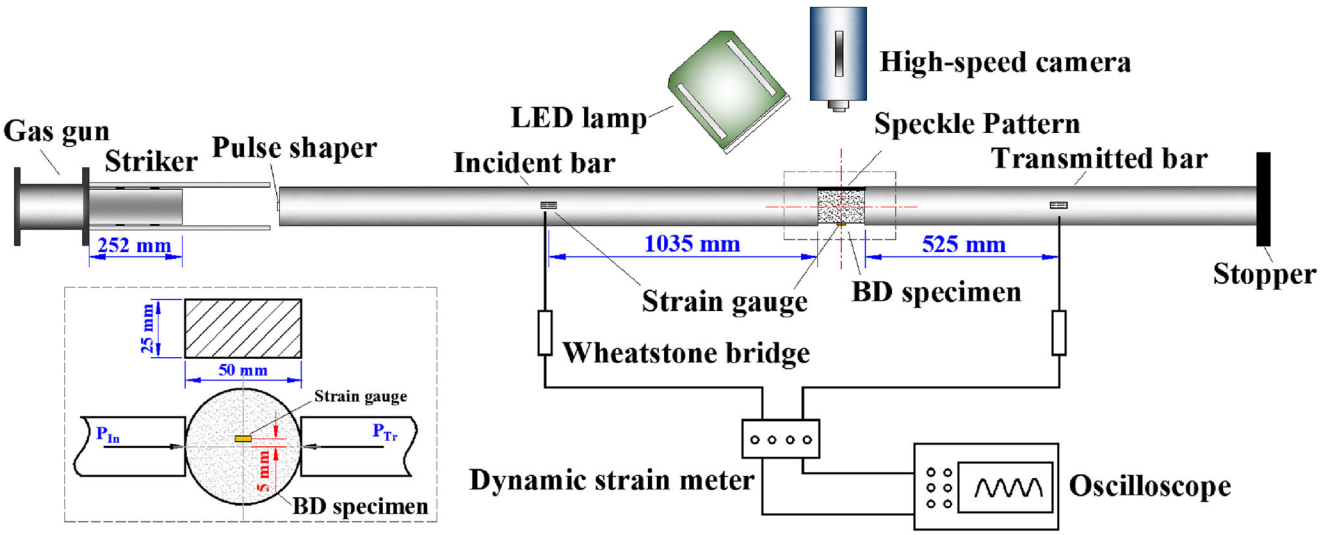

Fig. 1 Schematics of the split Hopkinson pressure bar (SHPB) system with the DIC technique

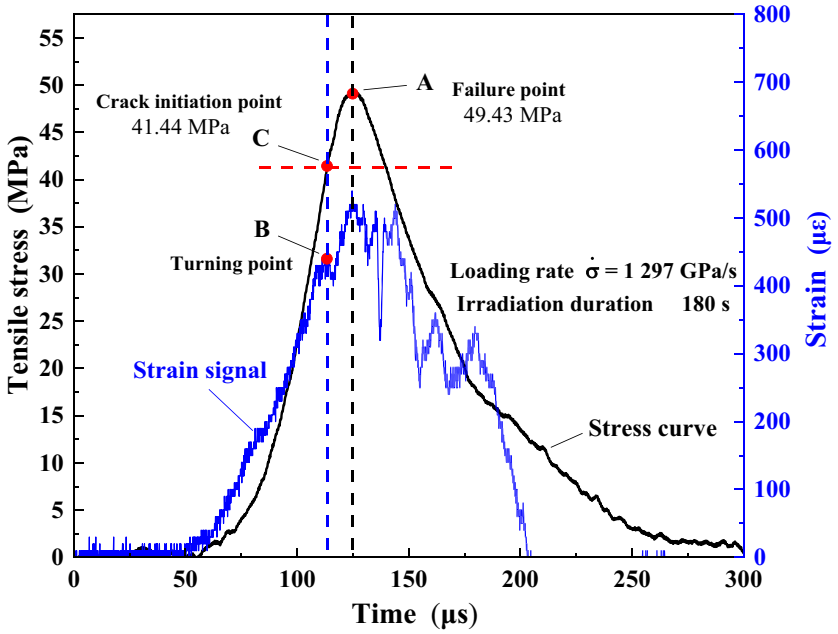

Fig. 2 A typical dynamic BD test for demonstrating the overload effect

solving the dynamic fracture energy is to determine the residue kinetic energy term K_f. Inspired by the work from Chen et al. [36], the digital strain gauge method was introduced to describe the displacement variation of the disc and infer the movement information of the fragments. Figure 4 shows the splitting velocity measurement of the two halves fragments for a typical test with a loading rate of 727 GPa/s and microwave irradiation duration of 180 s. As shown in Fig. 4(a), a virtual strain gauge A_0B_0 with a length of $l_d = 14$ mm is attached through the center of the disc along the diameter perpendicular to the loading direction. The displacement histories of the two symmetrical endpoints, A_0 and B_0, perpendicular to the loading direction (D_{xx}) are found to be very similar. The absolute value of the displacement component D_{yy} of B_0 is used for comparison. We differentiate the displacement value with time and the velocity histories of these two points can thus be acquired as depicted in Fig. 4(b). With a little discrepancy, one can still find that both the horizontal (V_{xx}) and the vertical (V_{yy}) velocities are almost identical during the overall dynamic loading and unloading process, indicating that the movements of the two halves of the disc are essentially symmetrical. Furthermore, the horizontal and vertical velocities exhibit completely different behaviors. Specifically, the change of V_{xx} remains synchronous with the dynamic tensile stress in the disc center (red line), whereas V_{yy} changes little at the early stage of loading but increases drastically after the time point corresponding to the turning point onset of the stress-time curve.

Considering the overload effect and the velocity variation of the fragments, four individual stages I-IV can be used to describe the failure process in Fig. 4(b). In stage I (segment OA) the disc deforms elastically, and the primary tensile crack initiates in the center of the disc at point A. In stage II (segment AC) the crack propagates outward to the edges of the disc and the vertical velocity of the particles rapidly increases with time. At the beginning of stage III (segment CD) the velocity V_{yy} reaches its maximum value (the terminal velocity V_t) and then significant fluctuations occur in this stage which are mainly attributed to the bending and shearing effects induced by subsequent loading. Secondary cracks are finally formed in this stage, which is reasonable because the terminal velocity of the fragments is relatively low (several meters per second) and cannot immediately escape the action range of the bars. Finally, in stage IV the velocity V_{yy} tends to be smoother and gradually decreases as time increases, indicating that the two halves of the disc completely flew out. Velocity V_{xx} has almost declined to zero since stage III, and thus the horizontal velocity component of the fragments can be neglected.

Moreover, two sets of symmetrical points A_1/A_1' and A_2/A_2' at the same height as A_0 were arranged as shown in Fig. 4(c), where the distance between neighboring points is set to 5 mm. One can see that the vertical velocities V_{yy} for these points appear to be almost identical, and thus the movements of two halves of the disc can be simply considered as translation. Furthermore, Fig.4(d) shows the displacement and vertical velocity variations of the digital strain gauge endpoints with different lengths. It is evident that the gauge length has a minimal effect on the vertical displacement and terminal velocity (the terminal velocity V_0 here is nearly twice that of V_{yy} in Fig. 4(b) and c because it refers to the relative value between the two endpoints). In fact, the increase of displacement induced by the elastic deformation is rather small compared with that caused by the opening of the crack. Consequently, the residue kinetic energy can be deduced

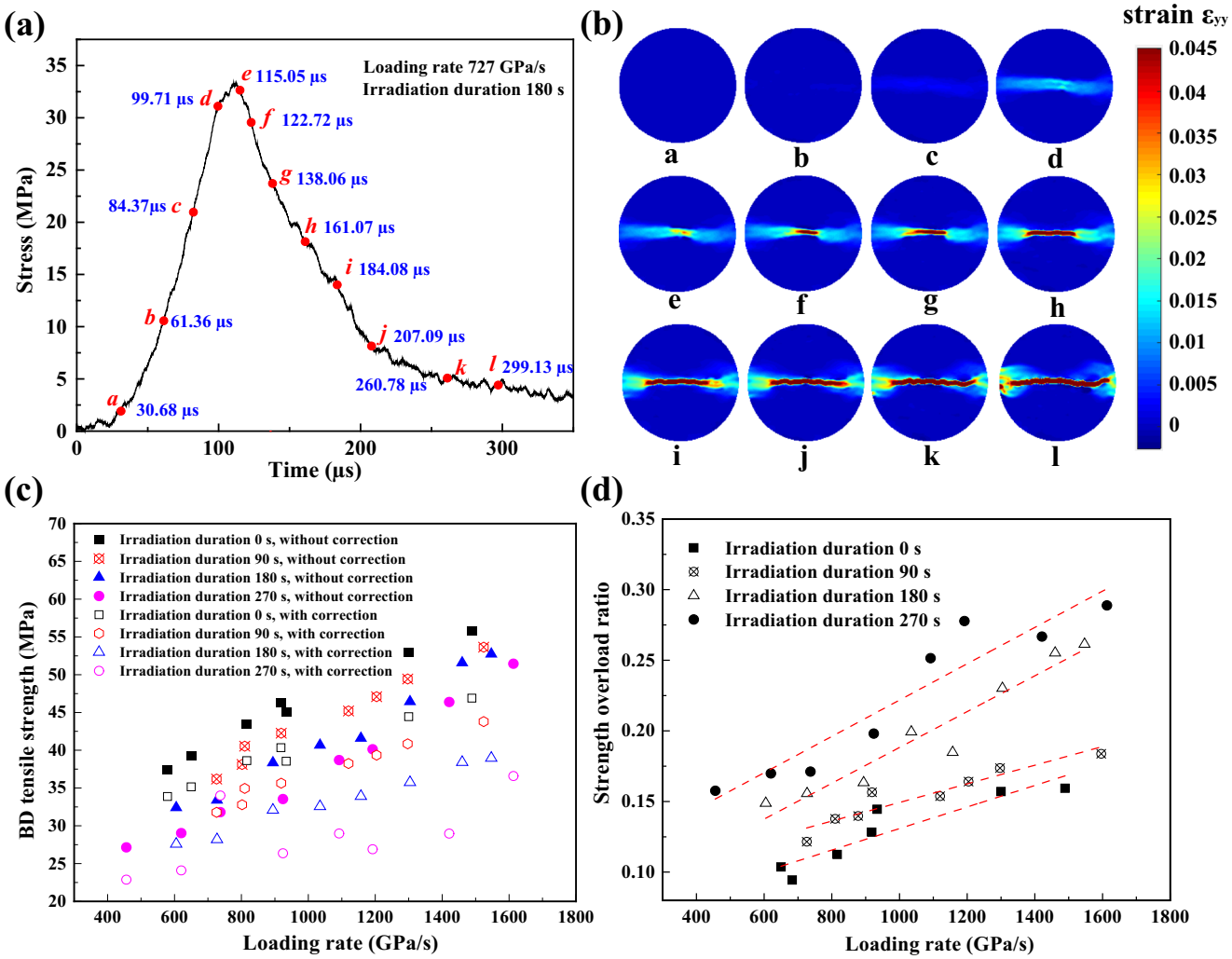

Fig. 3 The vertical strain distribution and strength characteristics (**a**) the stress versus time curve of the specimen (**b**) evolution of the vertical strain fields, in which snapshots a ~ l corresponds to the marked points in the stress-time curve (**c**) variations of the tensile strength with and without overload correction, and (**d**) variation of strength overload ratio of the dynamic tests

based on the velocity determined in Fig. 4, and the average fracture energy can then be calculated. It is also important to point out that the energy dissipation terms should be limited to stages I and II.

Figure 5 demonstrates the calculated average fracture energy versus the loading rate of FG rock for different irradiation durations. The fracture energy increases with the increase of the loading rate while decreasing with the increase of the irradiation duration. With the increase of the irradiation duration, more microcracks are generated along grain boundaries or cleavage planes of quartz and feldspar [9], together with the fact that the heating effect also deteriorates the binding capacity between the grains [12], thus making it much easier and faster for the tensile crack initiating and propagating throughout the specimen. The results are consistent with those in our previous work [23], in which the notched semi-circular bending (NSCB) method and laser gap gauge measurement were adopted to calculate the fracture energy.

Interestingly, we find that the effect of the microwave irradiation duration on average fracture energy is more evident at higher loading rates (> 800 GPa/s) than that at lower loading rates (< 800 GPa/s). The slope of the fracture energy with respect to the loading rate decreases with the increase of the irradiation duration. This phenomenon is similar to the results of dynamic fracture toughness of thermal-treated Laurentian granite concluded by Yin et al. [37]. This might be explained by the micro-failure mechanism in the dynamic test. It is noteworthy that the microwave irradiation can significantly enhance the density of the microcracks in the specimen, but the rock failure depends both on the microcrack density and the loading rate: when the loading rate is low, the crack has sufficient time to fully expand along the most optimal route [24, 38, 39], thus similar values of average fracture energy before the loading rate of 800 GPa/s are observed in Fig. 5. Whereas for the dynamic tests at higher loading rates, the loading durations are shorter, restraining the time for crack

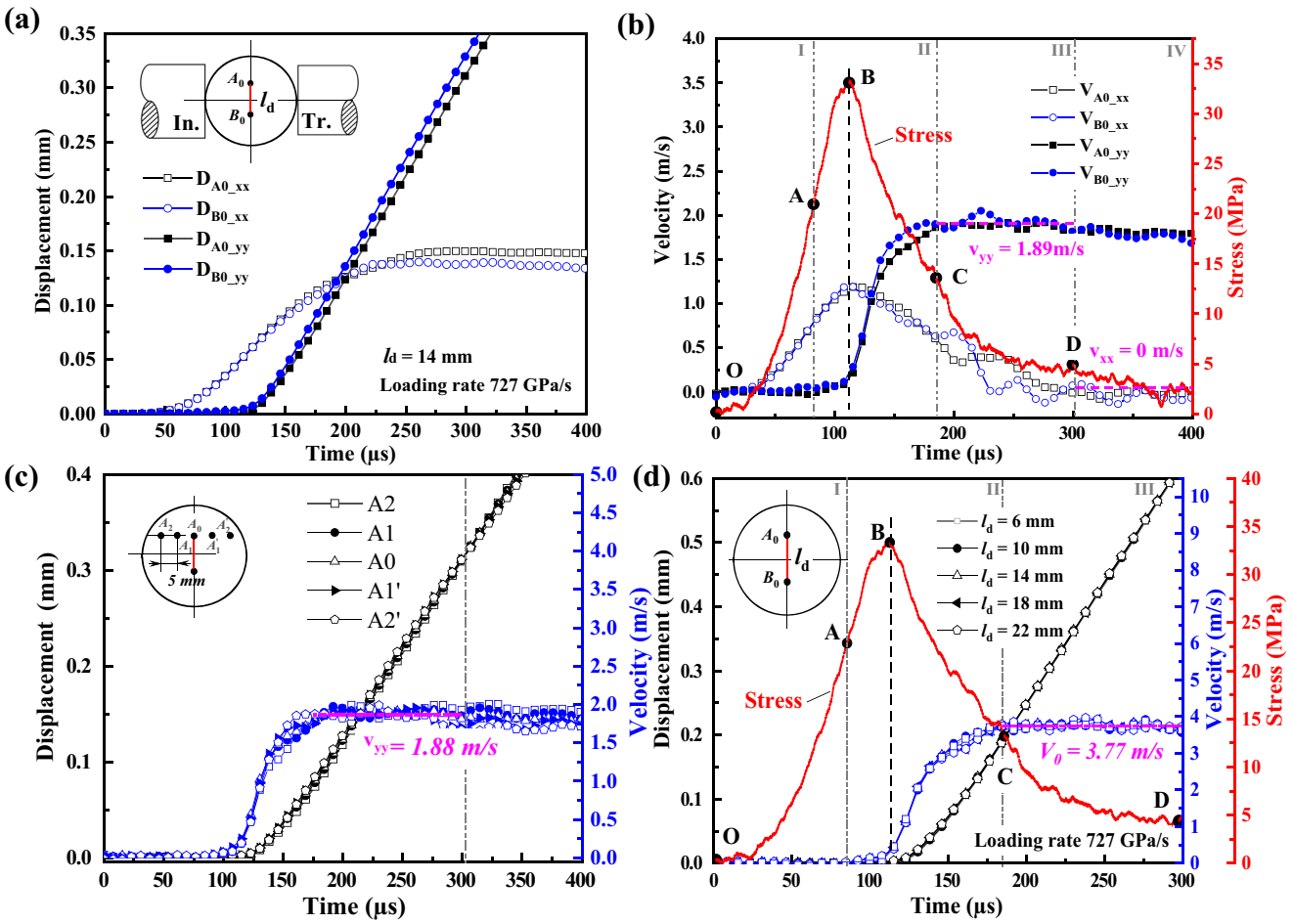

Fig. 4 Velocity measurement of the fragments for a typical test with the loading rate of 727 GPa/s and microwave irradiation duration of 180 s. (**a**) the displacement information of the endpoints A_0 and B_0 of DSG, (**b**) the velocity variation of the endpoints A_0 and B_0, (**c**) the displacements and velocities of the separate points, between which the distance is 5 mm

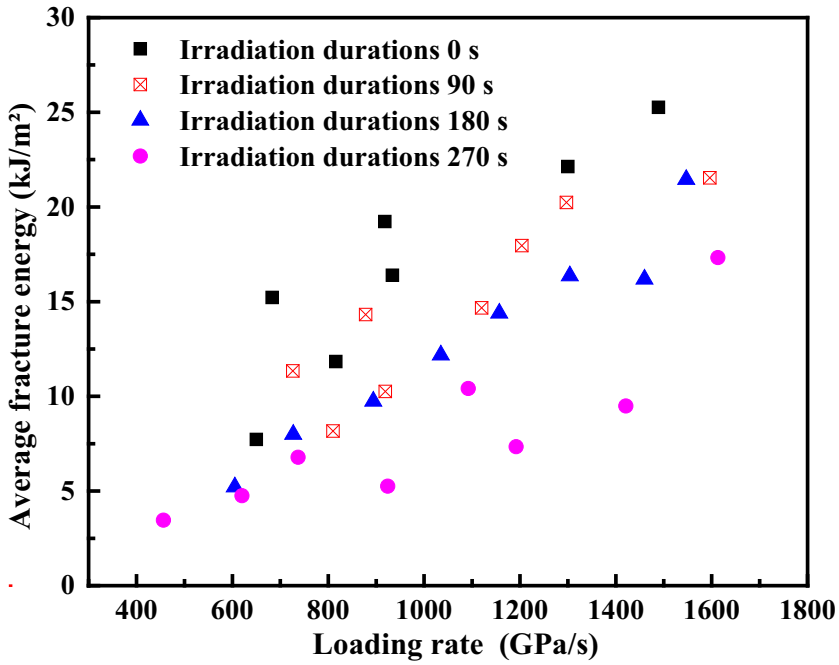

Fig. 5 The average fracture energy versus loading rate for different microwave irradiation durations

propagation and coalescence [40], thus more microcracks are involved in the failure process. As a result, the effect of microwave irradiation on the average fracture energy of FG is more evident at higher loading rates.

Conclusions

In summary, the dynamic tensile response of microwave damaged FG granite was studied using a SHPB system combined with the DIC technique. First, both the BD apparent and true tensile strengths exhibit an approximate linear increasing trend with the increase of the loading rate, whereas these strengths decrease with the increase of the microwave irradiation duration. The true tensile strength after overload correction is much lower than the apparent strength. Second, the movements of two halves of the disc were determined using the DIC analysis and the average fracture energy was calculated. The fracture energy increases with the loading rate while decreasing with the increase of the irradiation duration. Furthermore, the effects of the microwave irradiation duration on average fracture energy is more evident at higher loading rates than that at lower loading rates. The results in this study demonstrate that microwave irradiation can significantly weaken the tensile properties of the rock over a relatively short duration (several minutes), making it possible to design more efficient full-face tunnelling or other rock breaking equipment incorporating a microwave system.

Acknowledgements This work has been supported by the Natural Science Foundation of China (NSFC) under Grants #51879184 and #51704211. K.X. acknowledges financial support by the Natural Sciences and Engineering Research Council of Canada (NSERC) through the Discovery Grant #72031326.

Compliance with Ethical Standards

Conflict of Interest The authors declare that they have no conflict of interest.

References

1. Hartlieb P, Grafe B (2017) Experimental study on microwave assisted hard rock cutting of granite. BHM Berg-und Hüttenmännische Monatshefte 162(2):77–81. https://doi.org/10.1007/s00501-016-0569-0
2. Hassani F, Nekoovaght P (2011) The development of microwave assisted machineries to break hard rocks. In: Proceedings of the 28th International Symposium on Automation and Robotics in Construction (ISARC). Seoul: South Korea. pp 678–684. https://doi.org/10.22260/ISARC2011/0127
3. Hassani F, Nekoovaght PM, Gharib N (2016) The influence of microwave irradiation on rocks for microwave-assisted underground excavation. J Rock Mech Geotech Eng 8(1):1–15. https://doi.org/10.1016/j.jrmge.2015.10.004
4. Lu G-M, Feng X-T, Li Y-H, Zhang X (2019) The microwave-induced fracturing of hard rock. Rock Mech Rock Eng 52:3017–3032. https://doi.org/10.1007/s00603-019-01790-z
5. Kingman S, Corfield G, Rowson N (1999) Effects of microwave radiation upon the mineralogy and magnetic processing of a massive Norwegian ilmenite ore. Phys Sep Sci Eng 9(3):131–148. https://doi.org/10.1155/1999/57075
6. Nicco M, Holley EA, Hartlieb P, Kaunda R, Nelson PP (2018) Methods for characterizing cracks induced in rock. Rock Mech Rock Eng 51(7):2075–2093. https://doi.org/10.1007/s00603-018-1445-x
7. Lu G-M, Feng X-T, Li Y-H, Hassani F, Zhang X (2019) Experimental investigation on the effects of microwave treatment on basalt heating, mechanical strength, and fragmentation. Rock Mech Rock Eng 52:2535–2549. https://doi.org/10.1007/s00603-019-1743-y
8. Zheng Y, Zhang Q, Zhao J (2017) Effect of microwave treatment on thermal and ultrasonic properties of gabbro. Appl Therm Eng 127:359–369. https://doi.org/10.1016/j.applthermaleng.2017.08.060
9. Hartlieb P, Toifl M, Kuchar F, Meisels R, Antretter T (2016) Thermo-physical properties of selected hard rocks and their relation to microwave-assisted comminution. Miner Eng 91:34–41. https://doi.org/10.1016/j.mineng.2015.11.008
10. Lu G-m, Y-h L, Hassani F, Zhang X (2017) The influence of microwave irradiation on thermal properties of main rock-forming minerals. Appl Therm Eng 112:1523–1532. https://doi.org/10.1016/j.applthermaleng.2016.11.015
11. Sun W, Ling J, Huo J, Guo L, Zhang X (2013) Deng L (2013) dynamic characteristics study with multidegree-of-freedom coupling in TBM cutterhead system based on complex factors. Math Probl Eng 2013:1–17. https://doi.org/10.1155/2013/635809
12. Yao W, Xia K, Liu H-W (2018) Influence of heating on the dynamic tensile strength of two mortars: experiments and models. Int J Impact Eng 122:407–418. https://doi.org/10.1016/j.ijimpeng.2018.09.010
13. Song B, Sanborn B, Susan D, Johnson K, Dabling J, Carroll J, Brink A, Grutzik S, Kustas A (2019) Correction of specimen strain measurement in Kolsky tension bar experiments on work-hardening materials. Int J Impact Eng 132:103328. https://doi.org/10.1016/j.ijimpeng.2019.103328
14. Zhang QB, Zhao J (2014) A review of dynamic experimental techniques and mechanical behaviour of rock materials. Rock Mech Rock Eng 47(4):1411–1478. https://doi.org/10.1007/s00603-013-0463-y
15. Chu T, Ranson W, Sutton MA (1985) Applications of digital-image-correlation techniques to experimental mechanics. Exp Mech 25(3):232–244. https://doi.org/10.1007/BF02325092
16. Mellor M, Hawkes I (1971) Measurement of tensile strength by diametral compression of discs and annuli. Eng Geol 5(3):173–225. https://doi.org/10.1016/0013-7952(71)90001-9
17. Zhou Y, K-w X, Li X, Li H, Ma G, Zhao J, Zhou Z, Dai F (2012) Suggested methods for determining the dynamic strength parameters and mode-I fracture toughness of rock materials. Int J Rock Mech Min Sci 49:105–112. https://doi.org/10.1007/978-3-319-07713-0_3
18. Pan B, Qian K, Xie H, Asundi A (2009) Two-dimensional digital image correlation for in-plane displacement and strain measurement: a review. Meas Sci Technol 20(6):062001. https://doi.org/10.1088/0957-0233/20/6/062001
19. Gao G, Huang S, Xia K, Li Z (2015) Application of digital image correlation (DIC) in dynamic notched semi-circular bend (NSCB) tests. Exp Mech 55(1):95–104. https://doi.org/10.1007/s11340-014-9863-5

20. Blaber J, Adair B, Antoniou A (2015) Ncorr: open-source 2D digital image correlation Matlab software. Exp Mech 55(6):1105–1122. https://doi.org/10.1007/s11340-015-0009-1
21. Zhang Q, Zhao J (2013) Determination of mechanical properties and full-field strain measurements of rock material under dynamic loads. Int J Rock Mech Min Sci 60:423–439. https://doi.org/10.1016/j.ijrmms.2013.01.005
22. Xia K, Yao W, Wu B (2017) Dynamic rock tensile strengths of Laurentian granite: experimental observation and micromechanical model. J Rock Mech Geotech Eng 9(1):116–124. https://doi.org/10.1016/j.jrmge.2016.08.007
23. Li X, Wang S, Xu Y, Yao W, Xia K, Lu G (2020) Effect of microwave irradiation on dynamic mode-I fracture parameters of Barre granite. Eng Fract Mech 224:106748. https://doi.org/10.1016/j.engfracmech.2019.106748
24. Yao W, Xu Y, Wang W, Kanopolous P (2016) Dependence of dynamic tensile strength of longyou sandstone on heat-treatment temperature and loading rate. Rock Mech Rock Eng 49(10):3899–3915. https://doi.org/10.1007/s00603-015-0895-7
25. Sutton MA, Li N, Joy D, Reynolds AP, Li X (2007) Scanning electron microscopy for quantitative small and large deformation measurements part I: SEM imaging at magnifications from 200 to 10,000. Exp Mech 47(6):775–787. https://doi.org/10.1007/s11340-007-9042-z
26. Sutton MA, Li N, Garcia D, Cornille N, Orteu J-J, McNeill S, Schreier H, Li X, Reynolds AP (2007) Scanning electron microscopy for quantitative small and large deformation measurements part II: experimental validation for magnifications from 200 to 10,000. Exp Mech 47(6):789–804. https://doi.org/10.1007/s11340-007-9041-0
27. Efimov V (2009) The rock strength in different tension conditions. J Min Sci 45(6):569–575. https://doi.org/10.1007/s10913-009-0071-0
28. Perras MA, Diederichs MS (2014) A review of the tensile strength of rock: concepts and testing. Geotech Geol Eng 32(2):525–546. https://doi.org/10.1007/s10706-014-9732-0
29. Li D, Wong LNY (2013) The Brazilian disc test for rock mechanics applications: review and new insights. Rock Mech Rock Eng 46(2):269–287. https://doi.org/10.1007/s00603-012-0257-7
30. Fuenkajorn K, Klanphumeesri S (2010) Laboratory determination of direct tensile strength and deformability of intact rocks. Geotech Test J 34(1):97–102. https://doi.org/10.1520/GTJ103134
31. Fengchun J, Ruitang L, Xiaoxin Z, Vecchio KS, Rohatgi A (2004) Evaluation of dynamic fracture toughness KId by Hopkinson pressure bar loaded instrumented Charpy impact test. Eng Fract Mech 71(3):279–287. https://doi.org/10.1016/S0013-7944(03)00139-5
32. Dai F, Huang S, Xia K, Tan Z (2010) Some fundamental issues in dynamic compression and tension tests of rocks using split Hopkinson pressure bar. Rock Mech Rock Eng 43(6):657–666. https://doi.org/10.1007/s00603-010-0091-8
33. Yin T, Li X, Cao W, Xia K (2015) Effects of thermal treatment on tensile strength of Laurentian granite using Brazilian test. Rock Mech Rock Eng 48(6):2213–2223. https://doi.org/10.1007/s00603-015-0712-3
34. Zhou Z, Li X, Zou Y, Jiang Y, Li G (2014) Dynamic Brazilian tests of granite under coupled static and dynamic loads. Rock Mech Rock Eng 47(2):495–505. https://doi.org/10.1007/s00603-013-0441-4
35. Song B, Chen W (2006) Energy for specimen deformation in a split Hopkinson pressure bar experiment. Exp Mech 46(3):407–410. https://doi.org/10.1007/s11340-006-6420-x
36. Chen J, Guo B, Liu H, Liu H, Chen P (2014) Dynamic Brazilian test of brittle materials using the split Hopkinson pressure bar and digital image correlation. Strain 50(6):563–570. https://doi.org/10.1111/str.12118
37. Yin T, Li X, Xia K, Huang S (2012) Effect of thermal treatment on the dynamic fracture toughness of Laurentian granite. Rock Mech Rock Eng 45(6):1087–1094. https://doi.org/10.1007/s00603-012-0240-3
38. Curran D, Seaman L, Shockey D (1987) Dynamic failure of solids. Phys Rep 147(5–6):253–388. https://doi.org/10.1016/0370-1573(87)90049-4
39. Yao W, Xu Y, Xia K (2020) Damage evolution during rock pulverization induced by dynamic compressive loading. Journal of Geophysical Research: Solid Earth 125(5):e2020JB019388. https://doi.org/10.1029/2020jb019388
40. Wu B, Yao W, Xia K (2016) An experimental study of dynamic tensile failure of rocks subjected to hydrostatic confinement. Rock Mech Rock Eng 49(10):3855–3864. https://doi.org/10.1007/s00603-016-0946-8